Developmental Biology **229,** 307–318 (2001)
doi:10.1006/dbio.2000.0101, available online at http://www.idealibrary.com on IDEAL®

Spatial and Temporal Patterns of Cell Division during Early *Xenopus* Embryogenesis

Yasushi Saka[1,2] and James C. Smith[2]

Division of Developmental Biology, National Institute for Medical Research, The Ridgeway, Mill Hill, London NW7 1AA, United Kingdom

We describe the spatial and temporal patterns of cell division in the early *Xenopus* embryo, concentrating on the period between the midblastula transition and the early tailbud stage. Mitotic cells were identified using an antibody recognising phosphorylated histone H3. At least four observations are of interest. First, axial mesodermal cells, including prospective notochord, stop dividing after involution and may not divide thereafter. Second, cell division is more pronounced in the neural plate than in nonneural ectoderm, and the pattern of cell division becomes further refined as neurogenesis proceeds. Third, cells in the cement gland cease proliferation completely as they begin to accumulate pigment. Finally, the precursors of peripheral sensory organs such as the ear and olfactory placode undergo active cell proliferation when they arise from the sensorial layer of the ectoderm. These observations and others should provide a platform to study the relationship between the regulation of developmental processes and the cell cycle during *Xenopus* embryogenesis.

***Key Words: Xenopus;* cell cycle; cell division; gastrulation; morphogenesis; embryogenesis.**

INTRODUCTION

As our understanding of the mechanisms that govern the cell division cycle has advanced during the last quarter of the century (Nurse, 2000), it has become possible to study how cell proliferation is controlled at the molecular level during the development of multicellular organisms. In order to conduct such a study, it is essential to obtain either a precise developmental cell lineage or an accurate spatial and temporal map of embryonic cell division cycles. In *Caenorhabditis elegans,* embryonic blastomeres follow a fixed cell lineage (Sulston *et al.,* 1983). Embryos of *Drosophila melanogaster* do not have an invariant cell lineage, but clusters of synchronously dividing cells appear over the blastoderm surface shortly after cellularisation (Foe, 1989). These "mitotic domains" correspond to certain developmental fates and their positions and times of appearance are identical from embryo to embryo. Together, these observations indicate that cell-cycle control and the developmental programme are genetically linked.

Do mitotic domains exist in early vertebrate embryos, and might these reflect the fate map? In zebrafish embryos, three mitotic domains, with characteristic cell-cycle lengths, arise after the midblastula transition (MBT): the outer enveloping layer (EVL), the yolk syncytial layer (YSL), and the deep cells between the EVL and the YSL (Kane *et al.,* 1992). In contrast to *Drosophila,* however, there is no correlation between the zebrafish mitotic domains and the embryonic fate map. During gastrulation in the mouse embryo, after formation of the primitive streak, the embryo undergoes rapid growth that is attributed to the so-called "proliferative zone" in the anterior midline (Snow and Bennett, 1978). This observation and the others described above indicate that different species adopt different strategies to increase cell number during early stages of embryogenesis.

In *Xenopus laevis*, there have been many studies describing the synchronous cleavage of blastomeres prior to the midblastula transition (reviewed by Masui and Wang, 1998), and much is known about the underlying regulation of the cell-cycle machinery (Hartley *et al.,* 1996). At later stages, analyses have been restricted to the central nervous system. For example, it has been shown that neural tube closure and primary neurogenesis proceed normally without cell division after the onset of gastrulation (Harris and Hartenstein, 1991). If cell division is blocked, however, some abnormalities are observed such as a reduction in numbers of axons or dendrites and a disorganisation of the retina, presumably due to the reduction in primary neuron numbers (Harris and Hartenstein, 1991). These observa-

[1] To whom correspondence should be addressed. Telephone: +44 (0)1223 334131. Fax: +44 (0)1223 334134. E-mail: ys243@cam.ac.uk.

[2] Present address: Wellcome/CRC Institute, Tennis Court Road, Cambridge CB2 1QR, United Kingdom.

0012-1606/01 $35.00

tions indicate that although cell differentiation may occur independently of cell proliferation, development of fully functional organs requires normal cell division.

With the exception of this work and other work on cell division patterns during primary neurogenesis (Hartenstein, 1989), little is known about the global pattern of cell proliferation after MBT, when zygotic transcription starts and the cell cycle elongates (Newport and Kirschner, 1982a,b). In this paper we provide the first overall description of the spatial and temporal patterns of cell division in the early *Xenopus* embryo, concentrating on the period between the MBT and the early tailbud stage. To identify dividing cells, we employed an antibody recognising phosphorylated histone H3 (henceforth referred to as αPH3), which recognises cells in mitosis. Whole-mount staining of *Xenopus* embryos using this mitotic marker has produced several interesting observations. First, axial mesodermal cells become nonmitotic after involution and prospective notochord cells may not divide at all thereafter. Second, cell division is more pronounced in the neural plate than in nonneural ectoderm during neurula stages and becomes further refined as neurogenesis progresses. Third, cells in the future cement gland cease proliferation completely as they begin to accumulate pigment. Finally, the precursors of peripheral sensory organs such as the ear or olfactory placode undergo active cell proliferation when they form from the sensorial layer of the ectoderm. These observations and other results described below should serve as a platform to study the relationship between the regulation of developmental processes and the cell cycle during *Xenopus* embryogenesis.

MATERIALS AND METHODS

Embryonic Manipulations and Immunocytochemistry

Fertilisation, culture, and fixation of *Xenopus* embryos were as described (Tada *et al.*, 1997). Stock solutions of hydroxyurea (HU; Sigma) at 3 M in water and nocodazole (NOC; Sigma) at 10 mg/ml in DMSO were diluted in normal amphibian medium (NAM) immediately before use. For HU treatment, embryos were transferred to 1/10 NAM containing 30 mM HU 1 h after fertilisation and incubated at room temperature until control embryos reached stage 9. In the presence of HU, embryos continue to divide until maternal deoxynucleotide pools become exhausted around the time of MBT (Newport and Dasso, 1989). For NOC treatment, fertilised embryos were transferred to 1/10 NAM containing 10 μg/ml NOC at stage 8 and incubated for another 2 h at ambient temperature. Whole-mount immunostaining was carried out using an anti-phosphohistone H3 antibody (Upstate Biotechnology, 1 μg/ml). HRP-conjugated goat anti-rabbit IgG (H + L) (BioRad or Roche Molecular Biochemicals, 1:1000) was used as a secondary antibody. Embryos were dehydrated in methanol and cleared in benzyl benzoate/benzyl alcohol before examination (Figs. 3A and 5). For immunocytochemical sectioning, embryos were embedded in paraffin and sectioned at 10 μm. They were stained with methyl green (Fig. 3B) or by the Feulgen technique (Smith, 1993). For immunofluorescence microscopy, Cy3-conjugated goat anti-rabbit IgG (H + L) (Jackson ImmunoResearch Laboratories, 1:500) was used as a secondary antibody. Embryos were stained using DAPI (0.1–0.4 μg/ml in PBS), washed briefly in PBS, and then mounted in glycerol. They were observed using a Leica TCSNT confocal microscope system.

Image Acquisition

Immunocytochemical sections were observed using a Zeiss Axiophot microscope equipped with a JVC 3-CCD camera (JVC, model no. KY-F55B) and the images were acquired digitally by means of Image Grabber PCI system software (Neotech Ltd.). Images were processed with Adobe Photoshop™ (Adobe Systems Inc.). The public domain NIH Image program (U.S. National Institute of Health, available at http://rsb.info.nih.gov/nih-image/) was used to make composite images (Figs. 4 and 6) and to count nuclei (Table 1). Mitotic indices during gastrulation were determined by counting nuclei contained within 11–12 midsagittal sections for each embryo. For counting mitotic indices at stage 15, transverse sections in the trunks of two stained embryos were divided radially into six equal sectors, such that the dorsal-most sector contained the neural plate. The remainder of the ectoderm was regarded as nonneural ectoderm. The results are summarised in Table 2.

RESULTS

Visualisation of Mitotic Cells in the Xenopus Embryo

To visualise mitotic cells in *Xenopus* embryos, we used an αPH3 antibody. This antibody is highly specific for the phosphorylated form of the amino-terminus of histone H3 (serine 10), which is present from late G2 until telophase during the mitotic cell cycle (Hendzel *et al.*, 1997; Paulson and Taylor, 1982). The antibody has been shown to recognise mitotic chromosomes from a wide range of eukaryotes including human, *Tetrahymena*, *Drosophila*, and *C. elegans*.

To confirm that this antiserum also recognises mitotic chromosomes in *Xenopus*, embryos were fixed at stage 9 and stained by indirect immunofluorescence. Observation by confocal microscopy (Fig. 1) showed that αPH3 antibody-stained chromosomes strongly at metaphase (white arrowheads in A–C, and high magnification in D–F) as well as at prophase/prometaphase (green arrowhead) and at anaphase (arrow). Nuclei during other phases of the cell cycle were not stained or stained only weakly. To further confirm that αPH3 antibody recognises only mitotic nuclei in *Xenopus*, fertilised embryos were treated with either nocodazole, an inhibitor of microtubule assembly, or hydroxyurea, an inhibitor of ribonucleotide reductase (see Materials and Methods for details). These drugs have been shown to arrest cells at specific cell-cycle stages in *Xenopus;* nocodazole causes mitotic arrest (Clute and Masui, 1995) and HU blocks cells in S-phase (Newport and Dasso, 1989). As these drugs block cell division, blastomeres in nocodazole- or hydroxyurea-treated embryos are larger in size at the time

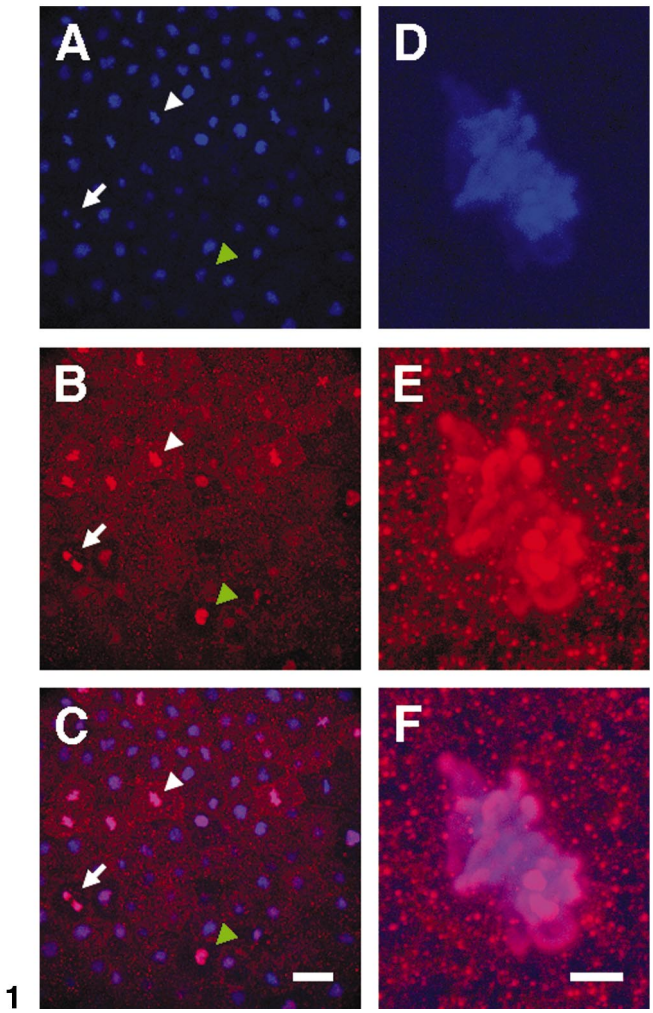

1

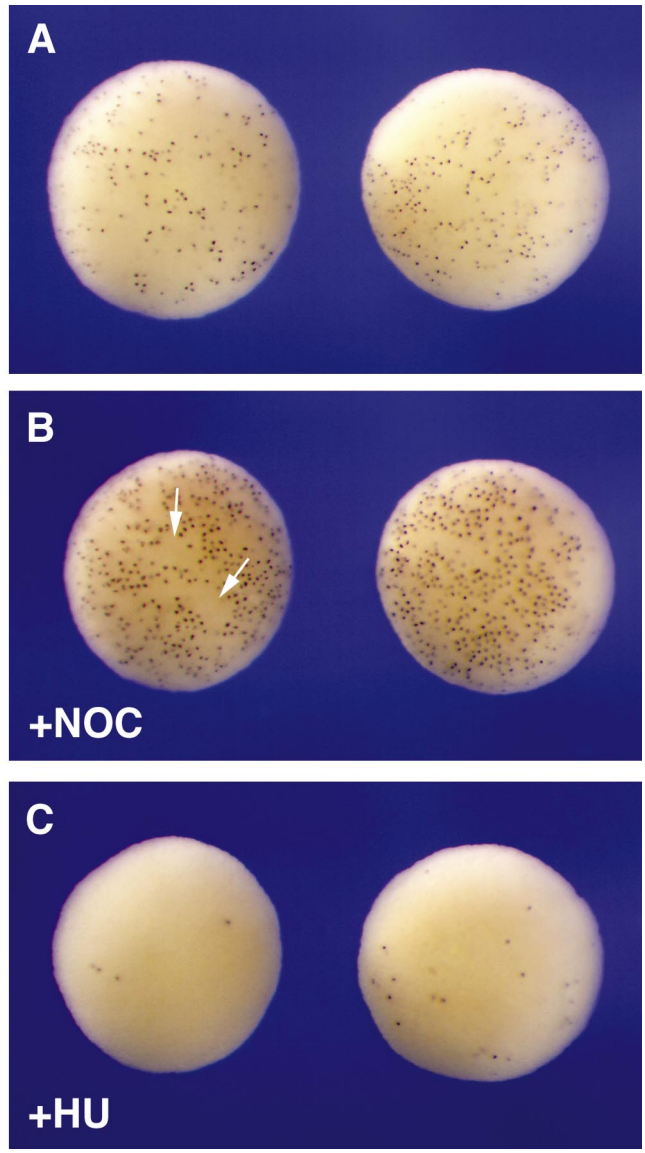

2

FIG. 1. Immunofluorescence microscopy of a *Xenopus* embryo stained with anti-phosphohistone H3 antibody (αPH3) at stage 9. The embryo was double-stained with the DNA dye DAPI (A and D, blue) and αPH3 (B and E, red) and observed with confocal microscopy. Merged images are shown in (C and F). (A–C) Images at low magnification and (D–F) at high magnification. Arrows in (A–C) indicate a cell in anaphase, white arrowheads a cell in metaphase, and green arrowhead a cell in prophase/prometaphase. In (D–F), individual condensed chromosome arms are clearly seen. Scale bar = 50 μm (A–C), or = 5 μm (D–F).

FIG. 2. Whole-mount immunostaining by αPH3 after treatment with nocodazole (NOC) and hydroxyurea (HU). Animal pole views of (A) control, (B) NOC-treated, and (C) HU-treated embryos at stage 9. Dark brown dots are αPH3-positive nuclei. A small population of cells in NOC-treated embryos was not stained by αPH3 antibody (2B, arrows), presumably because these cells had just completed the previous mitosis at the start of nocodazole application and had a cell-cycle period longer than the duration of the treatment (2 h).

of fixation than those in the control embryos (data not shown). The number of αPH3 antibody-stained nuclei increased significantly in nocodazole-treated embryos compared to those in the nontreated embryos (Figs. 2A and 2B). A small population of cells was not stained by αPH3 antibody (Fig. 2B, arrows), presumably because these cells had just completed the previous mitosis at the start of nocodazole application and had a cell-cycle period longer than the duration of the treatment (2 h). In contrast, hydroxyurea treatment caused a dramatic decrease in the number of αPH3 antibody-positive nuclei (Fig. 2C). The small number of αPH3-positive cells in these HU-treated

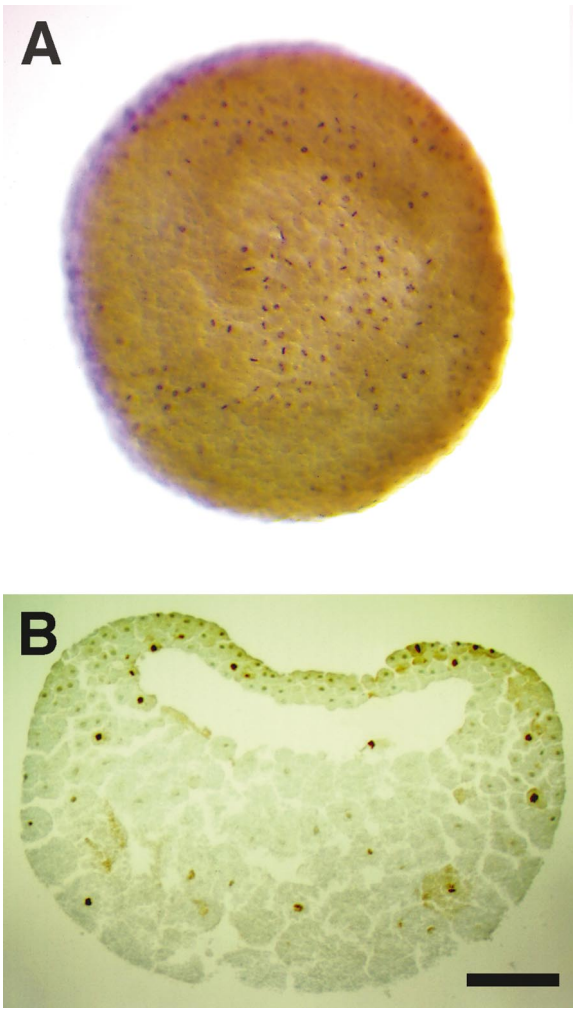

FIG. 3. *Xenopus* cell division pattern at stage 9. (A) Animal pole view of a whole embryo stained with αPH3 after clearing. Brown dots are mitotic nuclei. (B) Midtransverse section of a stained embryo. Mitotic nuclei appear as brown dots and other nuclei are light green.

embryos may have already completed DNA synthesis when the nucleotide pool became exhausted. These results confirmed that the αPH3 antibody detects only mitotic chromosomes in early *Xenopus* embryos.

The αPH3 reagent was then used to perform a series of whole-mount antibody stains to analyse the spatial and temporal patterns of cell division during early stages of *Xenopus* development. At least 10 embryos at each developmental stage were stained, dehydrated, and cleared for observation. We observed that patterns of cell divisions are very similar from embryo to embryo (data not shown). Some of the αPH3-stained embryos were subjected to histological sectioning for more detailed analysis. These results are presented below.

Spatiotemporal Pattern of Cell Division: Midblastula Transition to Stage 10

In the early cleavage stages of *Xenopus*, the cell-cycle length of each blastomere remains constant until the 10–12th cleavage. The transition from synchronous to asynchronous divisions occurs during the midblastula transition, but at different times in different regions of the embryo, with blastomeres closer to the vegetal pole losing synchrony a few cycles earlier than those in the animal pole (Boterenbrood and Narraway, 1983; Masui and Wang, 1998; Satoh, 1977). After MBT at stage 9, mitotic nuclei were distributed apparently randomly within the embryo (Figs. 1, 2A, and 3).

Spatiotemporal Pattern of Cell Division: Gastrula Stages

The first regional differences in the cell-division cycle were detected at gastrula stages, during which the overall mitotic index in the *Xenopus* embryo declines precipitously from 27.5% at stage 10.5 to 11.3% and 8.8% at stages 11 and 11.5, respectively (Table 1). Examination of sections of αPH3-stained embryos at stages 10.5–12.5 revealed no mitotic cells in the involuted dorsal axial mesoderm (Figs. 4D and 4F, highlighted in red). This observation indicates that cells of the prospective notochord may not divide from the midgastrula stage onward, a time which coincides with the demarcation of the notochord from paraxial mesoderm, but significantly precedes terminal differentiation and vacuolation at stage 23 (Hausen and Riebesell, 1991; Nieuwkoop and Faber, 1967). By contrast, mitotic cells were observed in the overlying ectoderm, in the anterior-most mesoderm (prospective prechordal plate) and in ventral mesoderm, as well as in the archenteron roof (Figs. 4C–4F).

Spatiotemporal Pattern of Cell Division: Neurula Stages

Whole-mount examination of *Xenopus* embryos at neurula stage 13 revealed mitotic cells distributed throughout the dorsal neurectoderm (Fig. 5A). By stage 15, as the neural

TABLE 1
Mitotic Indices in Gastrulating *Xenopus* Embryos

Stage	Sections counted (no. of embryos)	Mitotic nuclei	Total nuclei	% Mitotic cells
10.5	11 (1)	733	2668	27.5
11	34 (3)	1846	16,291	11.3
11.5	11 (1)	523	5977	8.8
12	33 (3)	1083	19,240	5.6
12.5	11 (1)	611	8224	7.4

Note. Determination of mitotic indices involved counting all nuclei contained within 11–12 midsagittal sections per embryo.

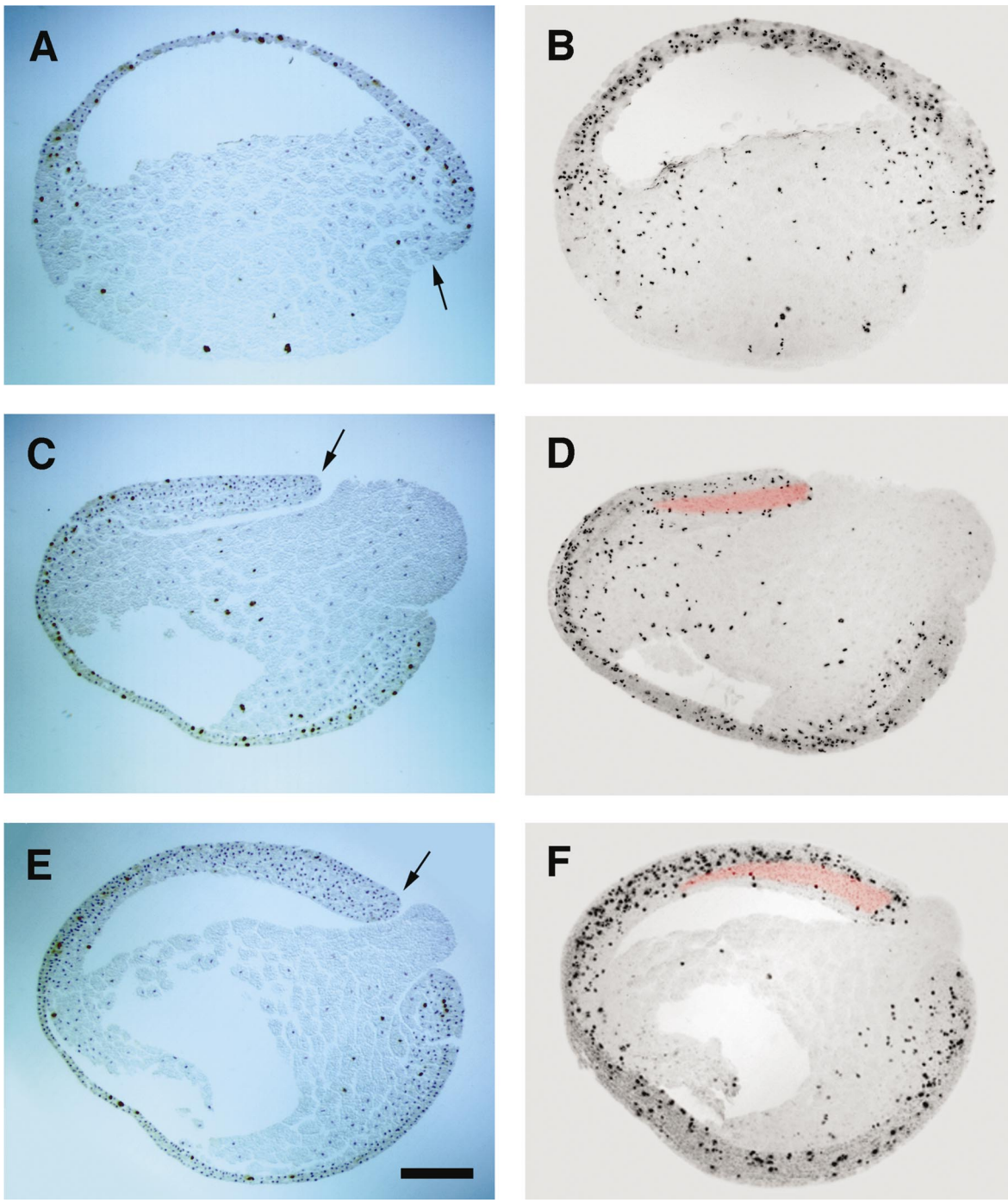

FIG. 4. Cell divisions detected by αPH3 in gastrula stage embryos. (A, C, and E) Sagittal sections of αPH3-stained embryos at stage 10.5, 11, and 12, respectively. Brown dots are mitotic nuclei and blue dots are nonmitotic nuclei. Arrows indicate dorsal lip. Scale bar is 200 μm. (B, D, and F) Composite images of 11 serial sagittal sections of a representative embryo at stages 10.5, 11, and 12, respectively. Mitotic nuclei appear as black dots. Dorsal axial mesoderm is highlighted in red; mitotic cells are absent. Note that due to distortion during sectioning, sections could not be registered with each other precisely.

plate converged dorsally and became narrower, stripes of mitotic cells appeared on both sides of the neural groove (Fig. 5B). Consistent with this observation, Hartenstein (1989) observed a wave of DNA replication, revealed by BrdU incorporation, moving from the lateral neural plate toward the dorsal midline between stages 13 and 15. At

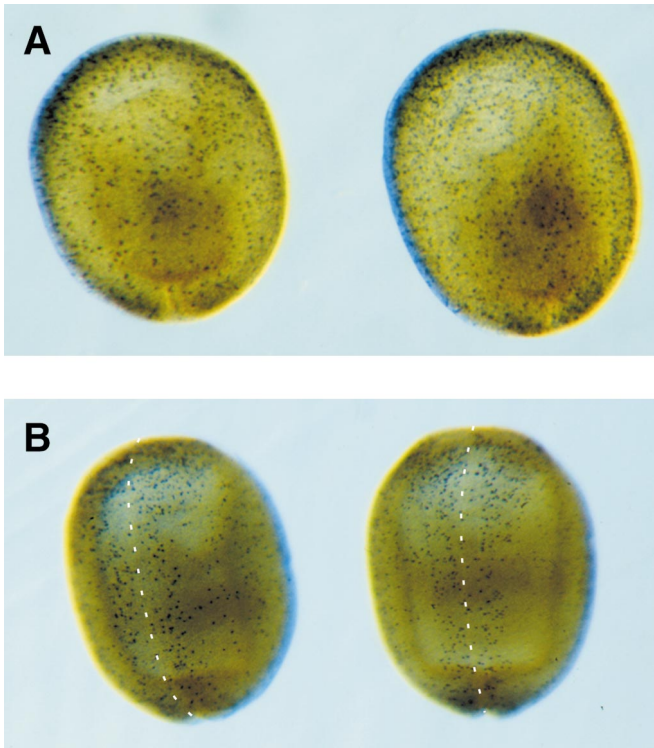

FIG. 5. Cell division patterns in early neurula embryos as detected by αPH3. Dorsal views of whole embryos, anterior to the top, at (A) stage 13 and (B) stage 15 are shown. Mitotic nuclei appear as brown dots. Dorsal midline is indicated in (B) by stippled lines. Mitotic cells become prominent on both sides of the midline at stage 15.

stage 15 the mitotic indices in the neural plate and the nonneural ectoderm of the trunk region were 6.2 and 3.9%, respectively (Table 2).

At stage 15, active cell proliferation was observed in the prospective brain and in the thickened layer of anterolateral neural plate that represents the eye vesicles (Fig. 6C). No cell division was observed in the presumptive notochord (see also Hissam and Belousov, 1983, 1984) and no mitoses were detected in somitic mesoderm, which is well demarcated from the lateral mesoderm by this time (Figs. 6B, 6E, and 6G). Mitotic figures were frequently observed in lateral and ventral mesoderm (Figs. 6A, 6F, 6G, and data not shown). The circumblastoporal collar was also active in proliferation compared with adjacent dorsal mesoderm, as is evident in a composite image of sagittal sections (Fig. 6B).

During stage 19, cell division was high in the central nervous system (Figs. 7A, 7C, and 7F) and, intriguingly, mitotic cells were frequently observed at the lateral edges of the somites (Figs. 7A and 7H, arrowheads). By contrast, no cell division was detectable at stage 18 in the epithelial layer of the ectoderm corresponding to the presumptive cement gland (Fig. 7I), and indeed mitotic figures were not detected in the cement gland thereafter. No such quiescence was observed at stage 15 (data not shown).

Spatiotemporal Pattern of Cell Division: Early Tailbud Stage 23

Mitotic figures in the central nervous system were detected predominantly in the cell layer facing the brain ventricle and central canal of the spinal cord (Figs. 8B–8E). Many mitotic figures were also observed in the ear placode, which arises through invagination of the sensorial layer of the epidermis, and in nearby neural crest cells (Figs. 8B, 8C, 8F, 8G, and 8H, arrows). Interestingly, when the olfactory placode became distinct as a thickening of the sensorial layer of epidermis anterior to the forebrain, cells here also showed active proliferation (Figs. 8D and 8E, arrowheads).

The anterior endoderm of the embryo gives rise to gill pouches and liver diverticulum (Graham and Morgan, 1966). Although cell density is higher in this region than in medial or posterior endoderm, there was no suggestion of an increased occurrence of cell division anteriorly (Figs. 8D, 8E, 8I, 8J, and 8K).

DISCUSSION

Our objective is to understand the relationship between patterns of cell division, morphogenesis, and differentiation in the early *Xenopus* embryo. We have used αPH3 as a marker of mitosis to examine the spatial and temporal patterns of cell division from the midblastula transition to the early tailbud stage. Our observations show that highly reproducible patterns of cell proliferation exist in early *Xenopus* embryos. Furthermore, there is a strong correlation between the early events of development and the regulation of the cell cycle, most notably in the suppression of cell proliferation in dorsal mesodermal cells during gastrulation.

TABLE 2
Mitotic Indices in Neural and Nonneural Ectoderm at Stage 15

	Sections counted[a]	Neural or nonneural[b]	Mitotic nuclei	Total nuclei	% Mitotic cells[c]
Embryo 1	8	Neural	38	629	6.0
		Nonneural	87	1926	4.5
Embryo 2	5	Neural	30	475	6.3
		Nonneural	42	1352	3.1

[a] Intervals between the counted sections are 50 μm for Embryo 1 and 100 μm for Embryo 2.

[b] Transverse sections in the trunk region were radially divided into six equal sectors and ectoderm in the dorsal-most sector was regarded as neural plate.

[c] Average mitotic indices for the two embryos are 6.2% for neural and 3.9% for nonneural ectoderm.

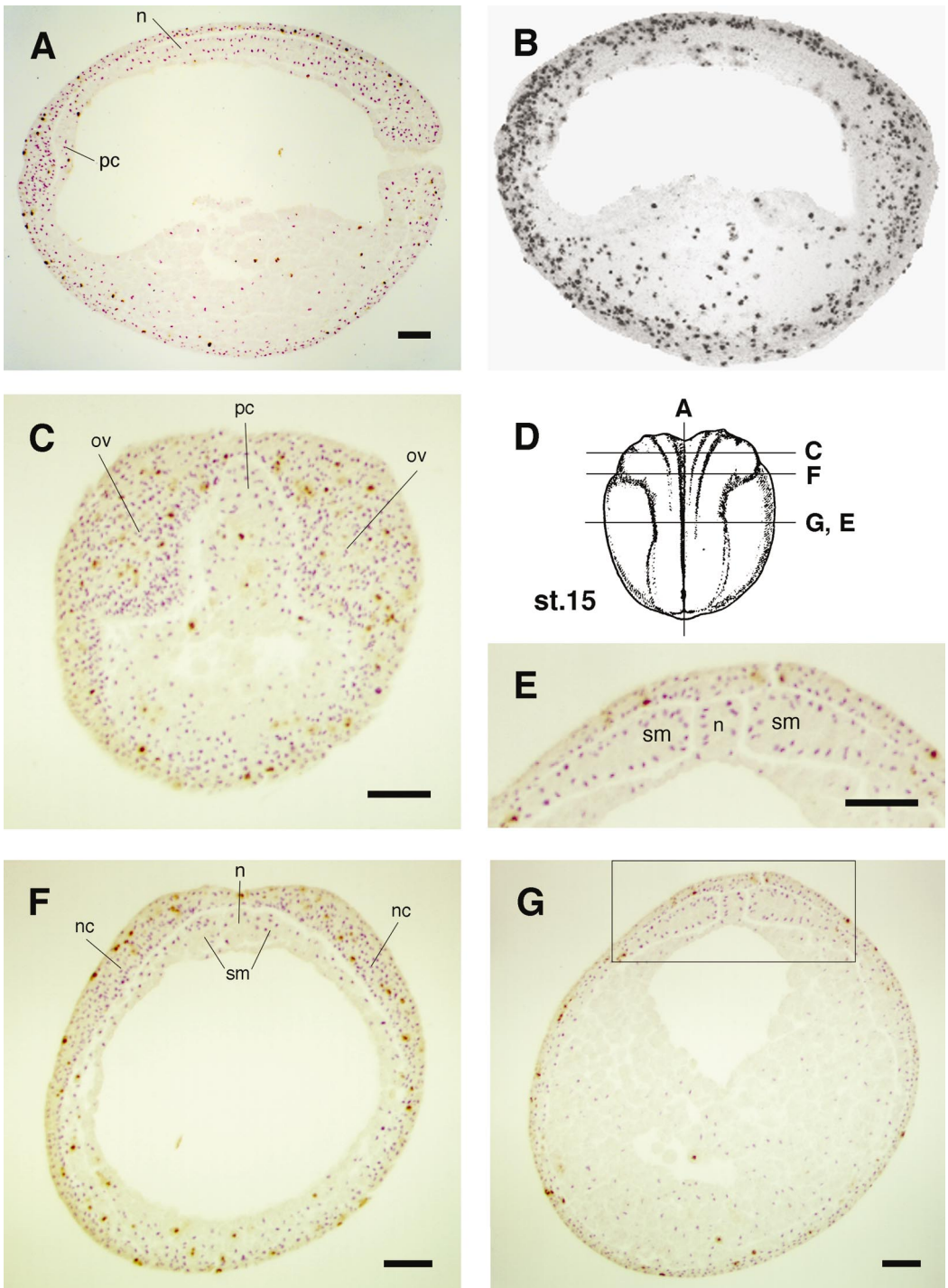

FIG. 6. Patterns of cell proliferation at stage 15. (A) A sagittal section, anterior to the left. (B) Composite images of 11 serial sagittal sections of a representative embryo. (C, F, and G) Transversal sections of αPH3-stained embryos. (D) Positions of sections as indicated in this schematic drawing of stage 15 embryo (dorsal view). The drawing of the embryo was taken from Nieuwkoop (1967). (E) Higher magnification of dorsal region as indicated by rectangle in (G). See text for details. Scale bar = 100 μm. Abbreviations: n, notochord; nc, neural crest; ov, optic vesicle; pc, prechordal plate; sm, somite.

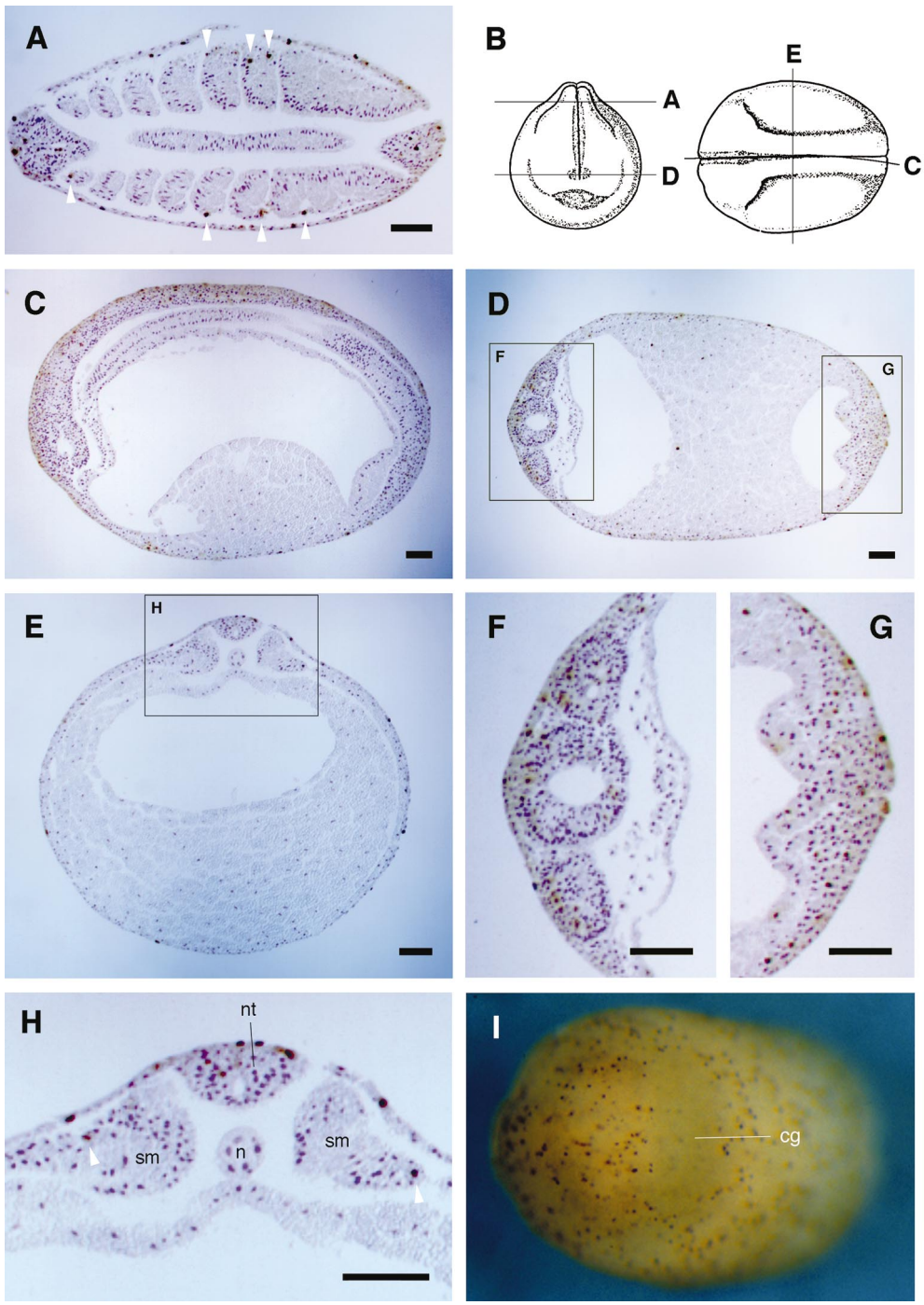

FIG. 7. Cell division patterns during late neurula stages. Mitotic nuclei are dark brown dots and the other nuclei are blue or purple. (A) Dorsal horizontal section of stage 20 embryo as indicated in (B). Notochord in the middle and six pairs of newly formed somites are seen. (B) Schematic representation of the positions of sections shown in this figure. The drawing of the embryo was taken from Nieuwkoop (1967). (C) Sagittal, (D) horizontal, and (E) midtransversal sections of stage 19/20 embryo. (F and G) Higher magnifications of head and tail region, respectively, as indicated by rectangles in (D). (H) Higher magnification of dorsal region indicated by rectangle in (E). (I) Anterior ventral view of αPH3-stained embryo at stage 18. No mitotic cells are present in cement gland region. Arrowheads in (A) and (H) indicate mitotic cells present in the lateral region of somites. Scale bar = 100 μm. Abbreviations; cg, cement gland; n, notochord; nt, neural tube; sm, somite.

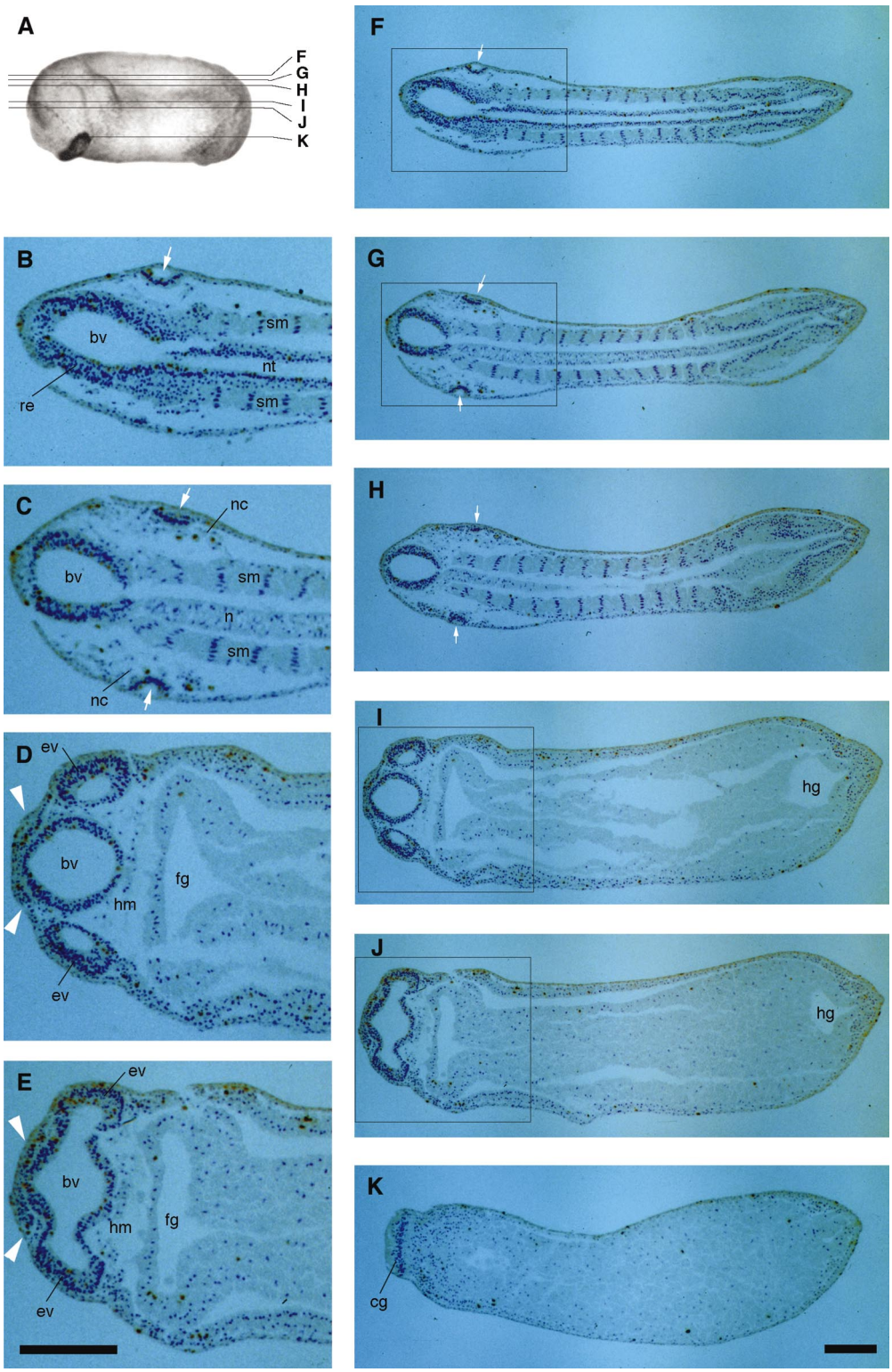

FIG. 8. Cell division patterns at early tailbud stage. (A) Schematic drawing of stage 23 embryo. Positions of horizontal sections in this figure are indicated. (B–K) Horizontal sections of αPH3-stained embryo at stage 23. (B–E) High magnifications of areas indicated by rectangles in (F, G, I, and J). Arrows indicate ear placodes and arrowheads olfactory placodes. Scale bar = 200 μm. Abbreviations; bv, brain ventricle; cg, cement gland; ev, eye vesicle; fg, foregut; hg, hindgut; hm, head mesenchyme; n, notochord; nc, neural crest; nt, neural tube; re, rhombencephalon; sm, somite.

Spatial–Temporal Pattern of Cell Division after MBT until the End of Gastrulation

During cleavage stages of *Xenopus* development, cells in the animal hemisphere of the embryo become smaller than those in the vegetal hemisphere. This phenomenon may be attributed both to unequal cytokinesis, with planes of cell division occurring away from the yolkier side of blastomeres, and to an earlier transition of synchronous to asynchronous cell divisions in the vegetal hemisphere at MBT (Masui and Wang, 1998). At stage 9, just after MBT, the αPH3 staining pattern indicates that mitotic figures are apparently randomly distributed (Figs. 1, 2A, and 3).

The increase in cell numbers during blastula stages may be significant in the regulation of gastrulation; Cooke (1973) showed that if cell division is blocked at the mid to late blastula stage, gastrulation movements are severely perturbed, suggesting that proper gastrulation requires a minimum number of cells.

Cooke (1973) also found, however, that if cell proliferation is inhibited after the onset of gastrulation, there is little effect on morphogenesis. This observation can now be viewed in light of our results which show that the dorsal mesodermal cells which drive gastrulation (Keller *et al.*, 1985) do not divide during gastrula and later stages anyway (Fig. 4). We note that in this respect the dorsal mesodermal cells contrast with anterior mesoderm, which is the first to involute and contains proliferating cells at all stages of gastrulation.

The lack of proliferation in dorsal mesodermal cells may be necessary for gastrulation to proceed normally. Recent results have demonstrated that inhibition of mitosis in prospective mesoderm is essential for normal gastrulation in *Drosophila* (Großhans and Wieschaus, 2000; Mata *et al.*, 2000; Seher and Leptin, 2000), and we plan to ask if the same is true in *Xenopus*.

Finally, the observation that the onset of gastrulation coincides with the appearance of cells in the G1 phase of the cell cycle (Frederick and Andrews, 1994) suggests that dorsal mesodermal cells are arrested in G1. In this regard, we note that $p27^{XIC1}$, a *Xenopus* homologue of the mammalian cyclin-dependent kinase inhibitor $p27^{Kip1}$, is expressed strongly in notochord and somites at the neurula stage, and that its expression pattern does not overlap with regions of high proliferation as revealed by BrdU incorporation (Hardcastle and Papalopulu, 2000). It will be interesting to see whether if $p27^{XIC1}$ is expressed in dorsal mesoderm to control the cell cycle during gastrulation.

Cell Proliferation in the Somites

In vertebrates, newly formed somites can be divided into medial and lateral compartments. The medial compartment gives rise to axial muscles and the skeleton while the lateral region forms muscles of the limbs and body wall. During avian somite patterning, this mediolateral specification is controlled by the opposing effects of BMP-4 secreted by lateral plate cells and noggin, a BMP-4 antagonist, produced by presumptive somite cells (Pourquié *et al.*, 1996; Tonegawa and Takahashi, 1998). Our observations indicate that only cells in the lateral compartment of somites undergo proliferation during somitogenesis (Figs. 7A and 7H). This is consistent with the observation that differentiation of lateral somitic cells is delayed compared with medial cells (Pourquié *et al.*, 1995) and it may be that additional proliferation of the lateral cells is required to produce enough cells to populate the entire hypaxial musculature. It is not known what controls proliferation in the lateral cells, although BMP-4 is one candidate for a mitogenic signal.

Pattern of Cell Proliferation in the Neural Plate

αPH3-staining during neurula stages showed that neural plate cells have higher mitotic activity than nonneuronal ectodermal cells (Fig. 5 and Table 2), suggesting that cell-cycle regulation differs in these two cell types. This higher mitotic activity may derive from a wave of cell division that sweeps from lateral to medial in the *Xenopus* neural plate, which causes lateral primary neuron precursors to become postmitotic earlier than medial ones (Hartenstein, 1989). Consistent with this idea, lateral, but not medial, longitudinal domains in the posterior neural plate do not incorporate BrdU during the midneurula stage (Hardcastle and Papalopulu, 2000).

Although this spatial and temporal pattern of cell proliferation might be important for the production of rows of different neuronal types (sensory, inter-, and motor neurons), further studies are needed to understand the role of the proliferation wave in primary neurogenesis. We note that primary neurogenesis can proceed without cell division (Harris and Hartenstein, 1991), suggesting that the role of cell proliferation is to obtain the correct number of primary neurons. Interestingly, cell death occurs among sensory neuron precursors shortly after the wave of mitosis (Hensey and Gautier, 1998), indicating that cell division and cell death are coordinated spatially and temporally during primary neurogenesis.

Cell Proliferation during Olfactory and Ear Placode Formation

The olfactory placodes appear around stage 21 while the otic placode starts to invaginate slightly later (Schlosser and Northcutt, 2000). Staining with αPH3 revealed that the appearance of these placodes was accompanied by cell proliferation (Figs. 8B–8E), suggesting that placode formation and cell proliferation are coordinated. In *Xenopus*, transplantation of ectoderm from different regions and stages has suggested that otic vesicle induction depends on the presumptive hindbrain (Gallagher *et al.*, 1996); if so, the same inductive signal might also induce cell proliferation. Similarly, an inductive signal from the developing forebrain may promote both olfactory placode formation and accompanying cell proliferation. However, we note again that otic

vesicle as well as lens formation can occur even when cell proliferation is blocked (Harris and Hartenstein, 1991). These results suggest that cell division is not required for the differentiation of these placodes, but may be necessary for formation of the functional organs or for achievement of the proper size. In the future it will be necessary to clarify the role of proliferation during development of these placodes.

Cement-Gland Formation and Cell-Cycle Regulation

The cement gland is a mucus-secreting organ derived from the most anterior region of the neurectoderm. At stage 18, but not stage 15, the cement gland primordium is visible as a sharply defined area of nonproliferating cells (Fig. 7I). Mitoses cannot be detected in the cement gland at later stages, either, when the cells became columnar and differentiate further (Fig. 8K), suggesting that cement gland cells exit the cell cycle around stage 18. Although the formation of cement gland and anterior neural tissue such as forebrain and midbrain are controlled by the homeobox gene *otx2* (Blitz and Cho, 1995; Pannese *et al.*, 1995), the timing of the cell-cycle exit before terminal differentiation must be controlled differently during the formation of these organs. The role of the cell-cycle exit in cement gland development, and the mechanism by which it occurs, await future investigation.

Conclusion: The Relationship between Patterns of Cell Division, Morphogenesis, and Differentiation in Xenopus Embryos

It is important during development that cells know when to divide and when not to divide, and the interpretation of experiments in which cell division is perturbed requires knowledge of what is the normal pattern of cell proliferation. One example of this point comes from the analysis of gastrulation in *Xenopus*. Inhibition of cell division by mitomycin C at the time of MBT blocks gastrulation because there are not enough cells for epiboly to be completed (Cooke, 1973). Later inhibition of cell cycle has a much more benign effect (Cooke, 1973; Harris and Hartenstein, 1991) because the involuted mesodermal cells that drive morphogenesis do not normally divide during gastrulation. Later inhibition of proliferation does have some effects, however, including a shortened axis, disorganised mesoderm (Cooke, 1973), and smaller eyes (Harris and Hartenstein, 1991). Interestingly, when HU-treated embryos were released from cell-cycle arrest, morphological abnormalities were exacerbated, suggesting that there is a critical period during which cell proliferation must occur if development is to proceed normally (Harris and Hartenstein, 1991). Such critical periods can be deduced from studies of the type presented here.

Finally, we note that most experiments examining the role of cell proliferation in *Xenopus* have involved inhibition of cell division. It will be interesting to test the consequences of forced cell proliferation in otherwise quiescent tissues such as axial mesoderm or the cement gland. This might be possible by overexpression of Cyclin E or E2F, which promote the G1 to S-phase transition (Nurse, 2000). Such an approach has been shown to be feasible in the *Drosophila* eye (Richardson *et al.*, 1995) and wing imaginal discs (Neufeld *et al.*, 1998).

ACKNOWLEDGMENTS

We are grateful to Wendy Hatton for sectioning and to Kate Sullivan and Stamatis Pagakis for confocal microscopy. We also thank Nancy Papalopulu for discussion and the referees for critical comments on the manuscript. This work is supported by the Medical Research Council and the Human Frontier Science Programme.

REFERENCES

Blitz, I. L., and Cho, K. W. Y. (1995). Anterior neurectoderm is progressively induced during gastrulation: The role of the *Xenopus* homeobox gene orthodenticle. *Development* **121,** 993–1004.

Boterenbrood, E. C., and Narraway, J. M. (1983). Duration of cleavage cycles and asymmetry in the direction of cleavage waves prior to gastrulation in *Xenopus laevis*. *Roux's Arch. Dev. Biol.* **192,** 216–221.

Clute, P., and Masui, Y. (1995). Regulation of the appearance of division synchrony and microtubule-dependent chromosome cycle in *Xenopus laevis* embryos. *Dev. Biol.* **171,** 273–285.

Cooke, J. (1973). Properties of the primary organization field in the embryo of *Xenopus laevis*. IV. Pattern formation and regulation following early inhibition of mitosis. *J. Embryol. Exp. Morphol.* **30,** 49–62.

Foe, V. E. (1989). Mitotic domains reveal early commitment of cells in *Drosophila* embryos. *Development* **107,** 1–22.

Frederick, D. L., and Andrews, M. T. (1994). Cell cycle remodeling requires cell-cell interactions in developing *Xenopus* embryos. *J. Exp. Zool.* **270,** 410–416.

Gallagher, B. C., Henry, J. J., and Grainger, R. M. (1996). Inductive processes leading to inner ear formation during *Xenopus* development. *Dev. Biol.* **175,** 95–107.

Graham, C. F., and Morgan, R. W. (1966). Changes in the cell cycle during early amphibian development. *Dev. Biol.* **14,** 439–460.

Großhans, J., and Wieschaus, E. (2000). A genetic link between morphogenesis and cell division during formation of the ventral furrow in *Drosophila*. *Cell* **101,** 523–531.

Hardcastle, Z., and Papalopulu, N. (2000). Distinct effects of XBF-1 in regulating the cell cycle inhibitor $p27^{XIC1}$ and imparting a neural fate. *Development* **127,** 1303–1314.

Harris, W. A., and Hartenstein, V. (1991). Neuronal determination without cell division in *Xenopus* embryos. *Neuron* **6,** 499–515.

Hartenstein, V. (1989). Early neurogenesis in *Xenopus:* The spatiotemporal pattern of proliferation and cell lineages in the embryonic spinal cord. *Neuron* **3,** 399–411.

Hartley, R. S., Rempel, R. E., and Maller, J. L. (1996). In vivo regulation of the early embryonic cell cycle in *Xenopus*. *Dev. Biol.* **173,** 408–419.

Hausen, P., and Riebesell, M. (1991). "The Early Development of *Xenopus laevis:* An Atlas of the Histology," Springer–Verlag, Berlin.

Hendzel, M. J., Wei, Y., Mancini, M. A., Van Hooser, A., Ranalli, T., Brinkley, B. R., Bazett-Jones, D. P., and Allis, C. D. (1997). Mitosis-specific phosphorylation of histone H3 initiates primarily within pericentromeric heterochromatin during G2 and spreads in an ordered fashion coincident with mitotic chromosome condensation. *Chromosoma* **106,** 348–360.

Hensey, C., and Gautier, J. (1998). Programmed cell death during *Xenopus* development: A spatio-temporal analysis. *Dev. Biol.* **203,** 36–48.

Hissam, J., and Belousov, L. V. (1983). Mitotic activity of the embryonic tissues of the clawed toad in the period of gastrulation and neurulation. *Ontogenez* **14,** 209–212.

Hissam, J., and Belousov, L. V. (1984). Spatial-temporal patterns of the cell cycles in embryos of the clawed toad during gastrulation and neurulation. *Ontogenez* **15,** 391–398.

Kane, D. A., Warga, R. M., and Kimmel, C. B. (1992). Mitotic domains in the early embryo of the zebrafish. *Nature* **360,** 735–737.

Keller, R. E., Danilchik, M., Gimlich, R., and Shih, J. (1985). The function and mechanism of convergent extension during gastrulation of *Xenopus laevis. J. Embryol. Exp. Morphol.* **89**(Supplement), 185–209.

Masui, Y., and Wang, P. (1998). Cell cycle transition in early embryonic development of *Xenopus laevis. Biol. Cell* **90,** 537–548.

Mata, J., Curado, S., Ephrussi, A., and Rørth, P. (2000). Tribbles coordinates mitosis and morphogenesis in *Drosophila* by regulating string/CDC25 proteolysis. *Cell* **101,** 511–522.

Neufeld, T. P., de la Cruz, A. F. A., Johnston, L. A., and Edgar, B. A. (1998). Coordination of growth and cell division in the *Drosophila* wing. *Cell* **93,** 1183–1193.

Newport, J., and Kirschner, M. (1982a). A major developmental transition in early *Xenopus* embryo. I. Characterization and timing of cellular changes at the midblastula stage. *Cell* **30,** 675–686.

Newport, J., and Kirschner, M. (1982b). A major developmental transition in early *Xenopus* embryos. II. Control of the onset of transcription. *Cell* **30,** 687–696.

Newport, J., and Dasso, M. (1989). On the coupling between DNA replication and mitosis. *J. Cell Sci.* **12**(Suppl.), 149–160.

Nieuwkoop, P. D., and Faber, J. (1967). "Normal Table of *Xenopus laevis* (Daudin)," North Holland, Amsterdam.

Nurse, P. (2000). A long twentieth century of the cell cycle and beyond. *Cell* **100,** 71–78.

Pannese, M., Polo, C., Andreazzoli, M., Vignali, R., Kablar, B., Barsacchi, G., and Boncinelli, E. (1995). The *Xenopus* homologue of Otx2 is a maternal homeobox gene that demarcates and specifies anterior body regions. *Development* **121,** 707–720.

Paulson, J. R., and Taylor, S. S. (1982). Phosphorylation of histones 1 and 3 and nonhistone high mobility group 14 by an endogenous kinase in HeLa metaphase chromosomes. *J. Biol. Chem.* **257,** 6064–6072.

Pourquié, O., Coltey, M., Bréant, C., and Le Douarin, N. M. (1995). Control of somite patterning by signals from the lateral plate. *Proc. Natl. Acad. Sci. USA* **92,** 3219–3223.

Pourquié, O., Fan, C. M., Coltey, M., Hirsinger, E., Watanabe, Y., Bréant, C., Francis-West, P., Brickell, P., Tessier-Lavigne, M., and Le Douarin, N. M. (1996). Lateral and axial signals involved in avian somite patterning: A role for BMP4. *Cell* **84,** 461–471.

Richardson, H., O'Keefe, L. V., Marty, T., and Saint, R. (1995). Ectopic cyclin E expression induces premature entry into S phase and disrupts pattern formation in the *Drosophila* eye imagianl disc. *Development* **121,** 3371–3379.

Satoh, N. (1977). "Metachronous" cleavage and initiation of gastrulation in amphibian embryos. *Dev. Growth & Differ.* **19,** 111–117.

Schlosser, G., and Northcutt, R. G. (2000). Development of neurogenic placodes in *Xenopus laevis. J. Comp. Neurol.* **418,** 121–146.

Seher, T. C., and Leptin, M. (2000). Tribbles, a cell-cycle brake that coordinates proliferation and morphogenesis during *Drosophila* gastrulation. *Curr. Biol.* **10,** 623–629.

Smith, J. C. (1993). Purifying and assaying mesoderm-inducing factors from vertebrate embryos. *In* "Cellular Interactions in Development—A Practical Approach" (D. Hartley, Ed.), pp. 181–204. Oxford University Press, Oxford.

Snow, M. H., and Bennett, D. (1978). Gastrulation in the mouse: Assessment of cell populations in the epiblast of tw18/tw18 embryos. *J. Embryol. Exp. Morphol.* **47,** 39–52.

Sulston, J. E., Schierenberg, E., White, J. G., and Thomson, J. N. (1983). The embryonic cell lineage of the nematode *Caenorhabditis elegans. Dev. Biol.* **100,** 64–119.

Tada, M., O'Reilly, M.-A. J., and Smith, J. C. (1997). Analysis of competence and of *Brachyury* autoinduction by use of hormone-inducible *Xbra. Development* **124,** 2225–2234.

Tonegawa, A., and Takahashi, Y. (1998). Somitogenesis controlled by Noggin. *Dev. Biol.* **202,** 172–182.

Received for publication August 17, 2000
Accepted November 9, 2000
Published online December 16, 2000